Journal of the Korean Ceramic Society (2021) 58:28–41
https://doi.org/10.1007/s43207-020-00100-6

REVIEW ARTICLE

Strategies for improving luminescence efficiencies of blue-emitting metal halide perovskites

G. Krishnamurthy Grandhi[1] · Ha Jun Kim[1] · N. S. M. Viswanath[2] · Han Bin Cho[1] · Joo Hyeong Han[1] · Seong Min Kim[1] · Won Bin Im[1]

Received: 17 September 2020 / Revised: 9 November 2020 / Accepted: 11 November 2020 / Published online: 3 December 2020

Abstract
Lead halide perovskites (LHPs) are suitable as the emissive layers in light-emitting diodes (LEDs). The external quantum efficiency of green LEDs based on LHPs is now over 20%. Nevertheless, the blue LHP LEDs lag behind the green ones in terms of efficiency. Photoluminescence (PL) quantum yield (QY) and stability of the NCs under various operating conditions are two major factors that influence the LED performance. Therefore, to promote the efforts towards achieving improved LED efficiencies, herein, we summarize several synthetic methods that produce blue-emitting LHP NC, followed by several approaches devised to boost their PL QYs up to near unity. Light-induced anion segregation is one of the limitations of using blue-emitting mixed-halide LHPs, which triggers the attention to single halide, quantum-confined LHP nanoplatelets (NPLs). Syntheses, structure, and luminescent properties of organic–inorganic and all-inorganic blue-emitting LHP NPLs are discussed elaborately. In the last portion, the luminescent properties of lead-free metal halides, which are of current interest, are discussed, followed by an outlook and future directions. In conclusion, our review discusses various literature attempts to obtain stable blue-emitting LHP NCs, which can be helpful in a better design of the blue-emitting LHP NCs towards various light-emitting applications.

Keywords Lead halide perovskites · Blue emission · Nanoplatelets · Lead-free perovskites

1 Introduction

Lead halide perovskites (LHPs) have not only become an exciting class of materials for thin-film-based photovoltaics and light-emitting diodes (LEDs), but also have made their mark in the field of colloidal semiconductor nanocrystals (NCs). LHPs were discovered towards the end of the nineteenth century; however, their potential was fully realized only by the end of the twentieth century. Research on LHPs has gained immense interest over the past few years owing to their unique characteristics such as long charge-carrier diffusion lengths and high absorption cross-sections. LHPs have found applications in lasers [1], gamma- and X-ray detection [2, 3], and photodetectors [4]. The efficiency of LHP-based solar cells has surpassed 20% over just a few years. LHPs display good electroluminescence (EL) properties, and their external quantum efficiency (EQE) has crossed 20% according to recent reports. Nano-sized LHPs offer interesting luminescent properties.

Although the first article on LHP NCs was on $MAPbBr_3$ NCs with a decent photoluminescence quantum yield (PLQY) in 2014 [5], the report by Protesescu et al. in 2015 piqued researchers' interest [6]. The fascinating feature of these NCs is their narrow-band and bright PL properties, which can be tuned from ultraviolet to the near-infrared wavelength regime by altering their halide composition, as shown in Fig. 1a–c for $CsPbX_3$ (X = Cl, Br, or I) NCs [6]. The near-unity PLQYs of these NCs were attributed to their defect tolerance. This means that the optical and electronic properties of the NCs are largely unaffected by their defects. In LHP NCs, efficient optical properties can be achieved without surface passivation or shell coating, unlike in conventional II–VI semiconducting NCs or GaAs NCs.

✉ Won Bin Im
imwonbin@hanyang.ac.kr

[1] Division of Materials Science and Engineering, Hanyang University, 222 Wangsimni-ro, Seongdong-gu, Seoul 04763, Republic of Korea

[2] School of Materials Science and Engineering, Chonnam National University, 77 Yongbong-ro, Buk-gu, Gwangju 61186, Republic of Korea

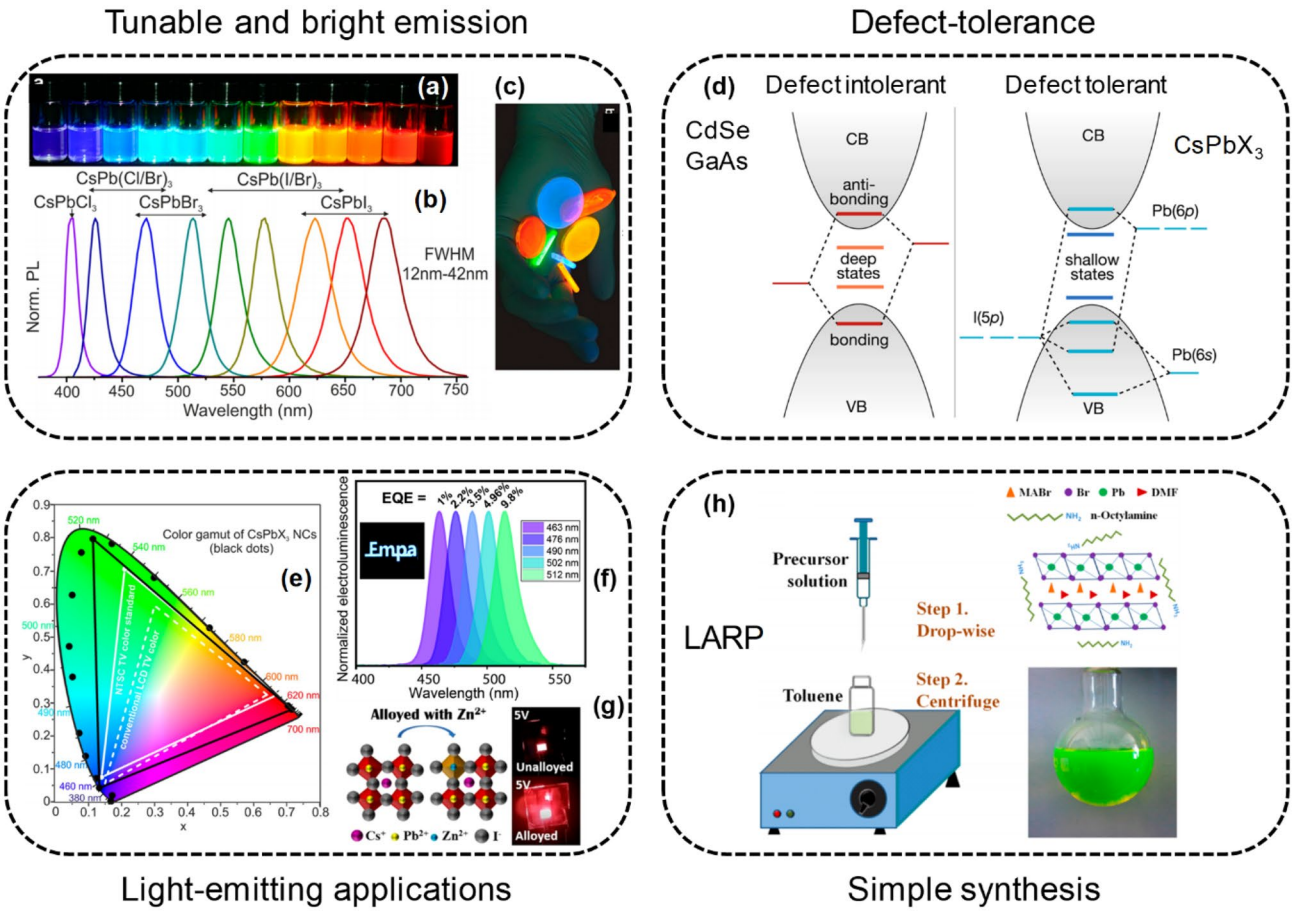

Fig. 1 Introduction to LHP NCs. **a** Colloidal solutions of $CsPbX_3$ NCs (X = Cl, Br, or I) in toluene under UV lamp ($\lambda = 365$ nm) and **b** the corresponding PL spectra. **c** Photograph (under UV light) showing bright luminescence from $CsPbX_3$ NCs-PMMA polymer monoliths achieved with Irgacure 819 as photoinitiator for polymerization. **d** Comparison of electronic structures of conventional semiconductors, such as, CdSe, GaAs, and InP (defect-intolerant) and LHPs (defect-tolerant). No photogenerated charge carriers can be trapped by defects in LHPs. **e** Comparison of CIE chromaticity coordinates (black data points) of the emission from $CsPbX_3$ NCs with the most common color standards (LCD TV (dashed white triangle) and NTSC TV (solid white triangle)). **f** EL spectra of $CsPb(Br_{1-x}Cl_x)_3$ NC LEDs. Inset shows the EL of the operating device with Empa emblem. **g** Unalloyed and Zn-alloyed $CsPbI_3$ structures and the pictures of respective LEDs. **h** The reaction system, precursor solution and process for ligand-assisted reprecipitation (LARP) technique as well as the photograph of colloidal $CH_3NH_3PbBr_3$ NC solution. **a**–**c** and **e** Reprinted with permission from Ref. [6] Copyright 2015, American Chemical Society. **d** Reprinted with permission from Ref. [7] Copyright 2017, American Chemical Society. **f** and **g** Reprinted with permission from Refs. [11, 13], respectively. Copyright 2019, American Chemical Society. **h** Reprinted with permission from Ref. [18] Copyright 2015, American Chemical Society

The defect energy levels exist entirely or partially (shallow traps) within either the valence band (VB) or the conduction band (CB) of the LHPs, as shown in Fig. 1d. However, conventional semiconducting NCs are defect-intolerant, which means the formation of defects affects their optical properties [7]. The defect-tolerant nature of LHPs has been attributed to their unconventional electronic structure (the bandgap is formed between antibonding orbitals) and very high formation energy of antisite and interstitial defects [8]. The other factor that facilitates efficient light emission from LHP NCs would be their bright triplet exciton [9].

Cd-based NCs have been exploited in optoelectronic applications such as color-conversion LEDs, and solid-state lighting [10]. They can cover over 100% of the NTSC (National Television System Committee) TV color standards. However, $CsPbX_3$ NCs comprise 140% of the NTSC standard, mainly in the red and green wavelength regions, as shown in Fig. 1e. Furthermore, the bright and narrow PL of the LHP NCs aided the fabrication of efficient LEDs, covering the entire visible regime. This has been achieved through various strategies such as appropriate surface passivation or ligand engineering and metal-ion doping (Fig. 1f, g) [11–13]. Furthermore, high-quality colloidal LHP NCs have been obtained by the hot-injection synthesis method. Precise control over their shapes and sizes was achieved [14, 15]. Chemical exfoliation [16] and ball-milling [17] were

also employed to synthesize high-quality LHP NCs. Owing to the labile (ionic) nature of their structure, room-temperature methods such as ligand-assisted reprecipitation (LARP) and reprecipitation can produce high-quality LHP NCs with very near unity PLQYs, as depicted in Fig. 1h [18–20].

Unlike for the red- and green-emitting LHP NCs, the optical properties, particularly the PLQY, reported for blue-emitting ones were lower [6, 21]. This low PL QY would have been a consequence of the relatively small sizes of the chloride ions and their resultant impact on the crystal structure or presence of more charge carrier trap states. This review article summarizes the various strategies for improving the luminescence efficiencies of the different blue-emitting perovskite NCs. We divide our review into five categories: (1) a brief overview of different ways of obtaining blue-emitting 3-D LHP NCs; (2) engineering methods for achieving high PLQY for these blue-emitting 3-D LHPs NCs; (3) structural and optical properties of quantum-confined organometal LHP nanoplatelets (NPLs); and (4) structural and optical properties of quantum-confined all-inorganic $CsPbX_3$ NPLs. In this section, we discuss different synthesis strategies and approaches for enhancing the NPL PLQYs. (5) The last portion introduces a few lead-free perovskite-like structures. At the end of the review, we have provided some insights into this field and tried to map its prospects.

2 Blue-emitting 3-D LHP NCs

Blue-emitting $CsPbCl_3$ or $CsPb(Cl/Br)_3$ was synthesized by mixing Pb, Cs, and halide precursors [6]. Because metal halides exhibit a higher ionic bonding tendency than metal chalcogenides, the post-synthetic chemical transformations of $CsPbX_3$ NCs were explored [22]. The blue-emitting $CsPbCl_3$ or $CsPb(Cl/Br)_3$ NCs were produced by partially or fully replacing the Br^- ions in the $CsPbBr_3$ lattice with Cl^- ions (Fig. 2a–c). A few suitable anion-exchange reagents were utilized, as shown in Fig. 2a. The crystal structure of $CsPbCl_3$ NCs gradually changed to $CsPbBr_3$ upon the addition of Br^- ions (Fig. 2b). The red shift in their bandgap further confirmed the anion-exchange process, as shown in Fig. 2c. The resultant NCs were not only emissive but also retained the sizes and shapes of the parent NCs. Cation doping into $CsPbX_3$ NCs also produced blue emission. Stable blue emission with a narrow FWHM was achieved by doping (alloying) $CsPbBr_3$ NCs with Al^{3+} ions (Fig. 2d, e) [23]. Al^{3+}:$CsPbBr_3$ NCs exhibited a blue-shifted PL emission with a maximum at 456 nm and a remarkable PLQY of 42%. The PL shift was attributed to the electronic doping by Al^{3+} ions as they introduced a new level (obtained by the hybridization of the Al-, Br-, and Pb-orbitals) in the bandgap of $CsPbBr_3$. A partial post-synthetic cation exchange of Pb^{2+} ions in $CsPbBr_3$ NCs with Sn^{2+}, Cd^{2+}, and Zn^{2+} led to a blue shift in the optical spectra, while preserving the original NC shape (Fig. 2f) [24]. The $CsPb_{1-x}M_xBr_3$ NCs, where $M = Sn^{2+}$, Cd^{2+}, and Zn^{2+}, displayed narrow blue emission with a PLQY > 50%. The PL blue shift was ascribed to the lattice contraction upon replacing a few Pb^{2+} ions with M^{2+} ions, as depicted in Fig. 2g. The blue shift was observed to scale linearly with the lattice shrinkage, independent of the cation introduced (Fig. 2h). This proves that the blue shift in the optical spectra was not a direct effect of the incorporated cations (they do not participate in the recombination/absorption process) but caused by the contraction of the host lattice, which widened the bandgap.

3 Bright and stable blue emission from the LHP NCs

Many attempts have been made to also improve the emission intensity and stability of LHP NCs. The cation doping in LHP NCs not only produced blue emission (as discussed in the introduction) but also enhanced their PL properties. Yong et al. reported all-inorganic violet-emitting $CsPb(Br/I)_3$ NCs with near-unity PLQYs by engineering the local order of the host lattice using Ni^{2+} doping, as shown in Fig. 3a [25]. The emission intensity of blue-emitting $CsPbCl_3$ NCs was also enhanced multifold via Ni^{2+} doping. Density functional theory calculations showed that the energy levels around the bandgap of $CsPbCl_3$ NCs are attributable to Pb and Cl atoms, whereas Cs atoms have negligible influence. Furthermore, a defect level exists in the bandgap of undoped $CsPbCl_3$ with Cl vacancies (Fig. 3b). These halide-induced defects would be the main reason for the low PLQYs of the blue-emitting NCs. Ni^{2+} doping eliminated the defect levels present inside the host bandgap, as shown in Fig. 3c, leading to enhanced emission intensities. The elimination of defects upon doping was verified by time-resolved PL spectroscopy. In this case, the PL decay curves show that the contribution of the fast-decay components (corresponding to non-radiative recombination) was diminished upon Ni^{2+} doping (Fig. 3d) [25]. Ni^{2+} doping also improved the stability and PL intensity of green-emitting LHP NCs [26]. Similarly, post-synthetic Cd^{2+} doping increases the PLQY of blue- and violet-emitting LHP NCs to near unity by removing the nonradiative defect states in the host bandgap [27]. Other transition metal ions such as Mn^{2+} and Cu^{2+} were also utilized to boost the emission characteristics of $CsPbCl_3$ and $CsPb(Cl/Br)_3$ NCs [28–31]. Figure 3e displays the PL spectra of Mn-doped and undoped NCs. Whereas undoped NCs exhibit excitonic emission only, Mn-doped NCs display both exciton emission as well as the emission band (~600 nm), corresponding to Mn-related recombination [28]. The blue emission was substantially increased in Mn-doped NCs, attributed to doping-induced removal of structural defects.

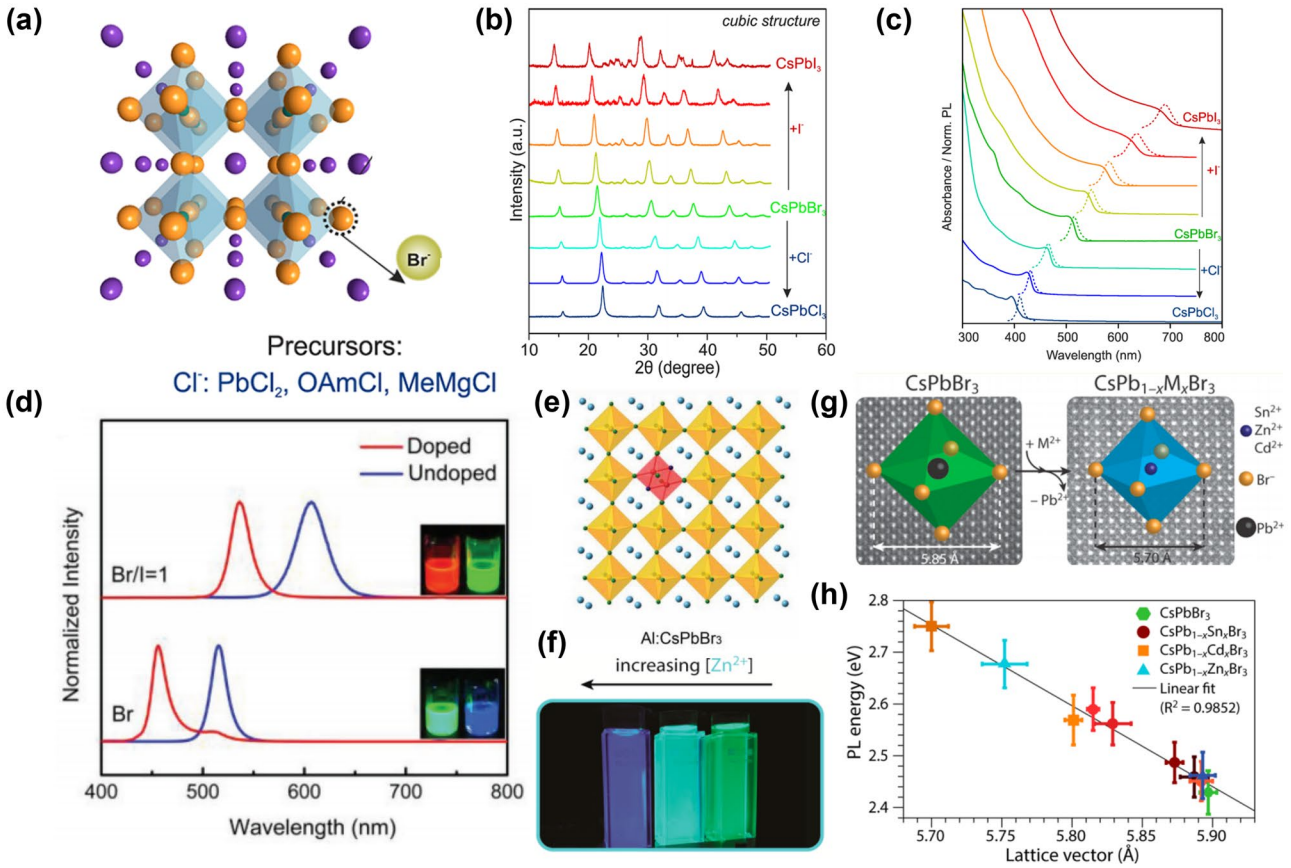

Fig. 2 Different ways of producing blue-emitting LHP NCs. **a** $CsPbBr_3$ crystal structure and a catalog of anion-exchange reagents. Evolution of the **b** powder XRD patterns and **c** optical absorption (solid lines) and PL (dashed lines) spectra of $CsPbBr_3$ NCs with increasing quantities of $PbCl_2$ or PbI_2, the exchanging halide sources. **d** PL spectra of Al-doped and undoped $CsPbBr_3$ and $CsPb(Br/I)_3$ NCs. Insets show the samples under UV excitation. **e** Schematic showing the Al bound to host lattice constituents in cluster form. **f** Parent $CsPbBr_3$ NCs (right vial) and product NCs after reaction of $CsPbBr_3$ NCs with increasing concentrations of $ZnBr_2$. **g** Illustration of post-synthetic partial Pb^{2+} cation exchange in $CsPbBr_3$ NCs by Sn^{2+}, Cd^{2+}, and Zn^{2+}. **h** PL energy as a function of the lattice vector in doped $CsPb_{1-x}M_xBr_3$ (M = Sn, Cd, or Zn) NCs obtained by the post-synthetic Pb^{2+} cation exchange. **a**–**c** Reprinted with permission from Ref. [22] Copyright 2015, American Chemical Society. **d** and **e** Reprinted with permission from Ref. [23] Copyright 2017, John Wiley and Sons. **f**–**h** Reprinted with permission from Ref. [24] Copyright 2017, American Chemical Society

Samanta and co-workers demonstrated that $CuCl_2$ addition during the synthesis of $CsPbCl_3$ NCs produced blue- and violet-emitting Cu-doped NCs with near-unity PLQY, as shown in Fig. 3e [29]. The remarkable PL enhancement was ascribed to the prevention of lead halide octahedral distortion and surface passivation by excess Cl^- ions. Transient absorption spectroscopy confirmed the suppression of the charge carrier trapping process in Cu-doped NCs. Another report showed that Cu^{2+} doping imparted very high thermal stability to the blue-emitting LHP NCs in addition to bright emission. Extended X-ray absorption fine structure (EXAFS) measurements revealed that small-sized Cu^{2+} dopant ions induced contraction of the host lattice, which altered the lattice formation energy and thereby improved the material stability [30]. Dual-surface passivation led to a large enhancement (60 times) in the PLQY of $CsPbCl_3$ NCs, as shown in Fig. 3g [32]. YCl_3 filled the Pb–Cl ion pair defects and passivated the surface Pb atoms. In other words, YCl_3 treatment led to efficient passivation of the NC surface defects and consequent suppression of the formation of nonradiative recombination centers on the surface. YCl_3 not only eliminated the surface defects but also preserved the PL properties for longer durations, as shown in Fig. 3h [32]. Furthermore, filling the chloride vacancies with thiocyanate molecules also provided near unity PLQY for $CsPb(Br/Cl)_3$ NCs [33]. Stable and bright blue emission from the LHP NCs was also achieved through the alternative strategies. Blue-emitting $CsPbBr_3$–silica composites were produced with PLQY of 72% via bandgap engineering [34]. LHP NC–silica composites with distinct emission colors were utilized for fabricating white LEDs [34]. Anion-exchange between $CsPbCl_3$ and Cs_4PbBr_6 NCs produced

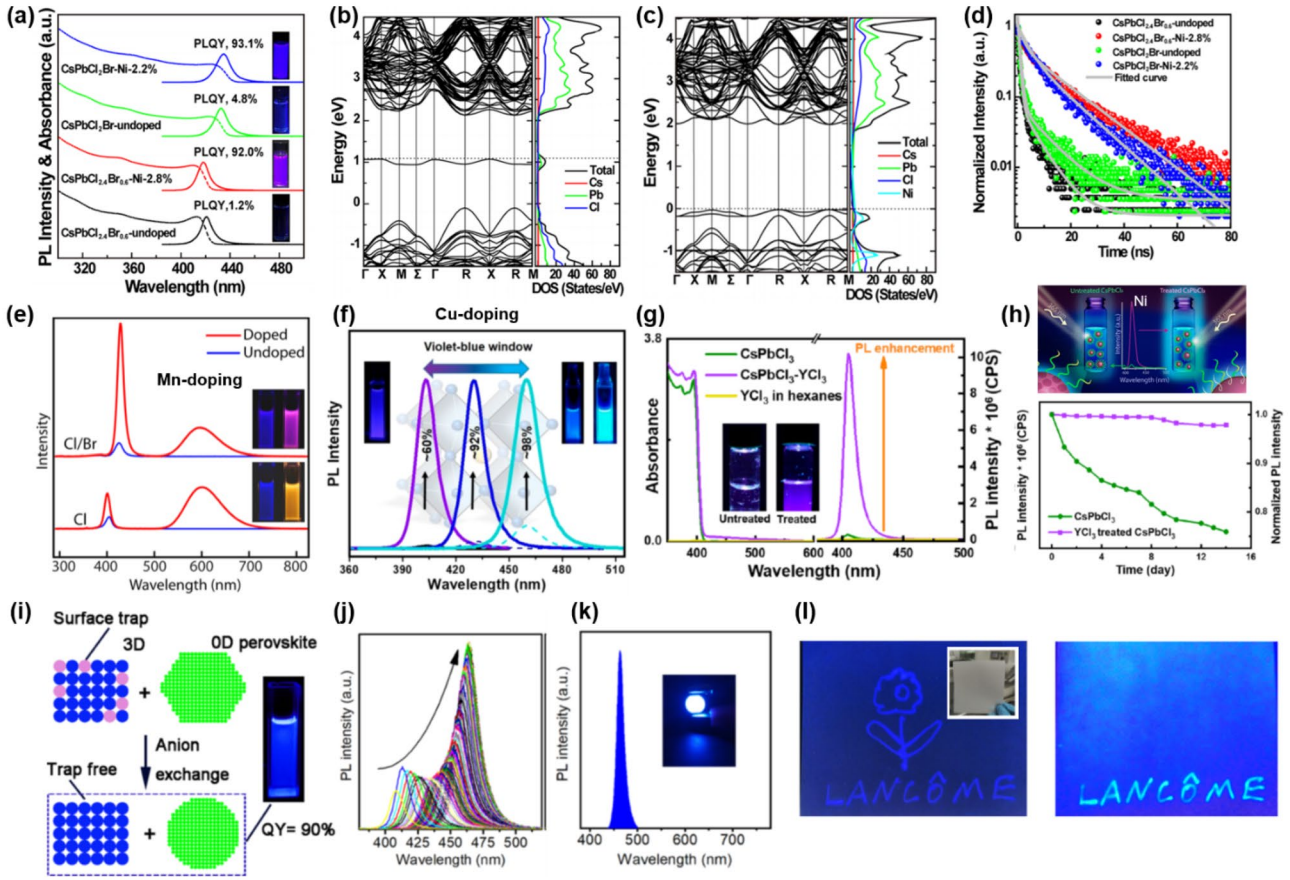

Fig. 3 Strategies for boosting blue-emission intensity of LHP NCs. **a** Absorption and PL spectra of undoped and Ni^{2+}-doped $CsPb(Cl,Br)_3$ NCs. Band structure and density of states (DOS) of **b** undoped $CsPbCl_3$ with a Cl vacancy and **c** Ni-doped $CsPbCl_3$ without any defect. The horizontal dotted lines represent the Fermi levels. **d** PL decay traces of undoped and Ni-doped $CsPb(Cl,Br)_3$ NCs. Comparison of PL spectra of Mn-doped **e** and Cu-doped **f** with the undoped $CsPbCl_3$ and $CsPb(Cl/Br)_3$ NCs. **g** Absorption and PL spectra of the $CsPbCl_3$ NCs before and after YCl_3 surface passivation. **h** Variation of relative PL intensity as a function of time for pristine NCs and YCl_3-passivated NCs after exposure to ambient conditions. **i** Graphic of the anion-exchange process between $CsPbCl_3$ and Cs_4PbBr_6 NCs and **j** the corresponding PL spectra. **k** PL spectrum of UV LED chip coated with the sample (**i**) (inset is the photograph of LED operated at 20 mA). **l** Trademark pattern of the Lancôme written by security inks under UV light and decryption information of the trademark pattern after being treated with water. Inset: photograph of the painting paper under ambient light. Insets of **a**, **e**, **f**, and **g** are photographs of the samples under UV excitation. **a–d** Reprinted with permission from Ref. [25] Copyright 2018, American Chemical Society. **e** Reprinted with permission from Ref. [28] Copyright 2016, American Chemical Society. **f** Reprinted with permission from Ref. [29] Copyright 2019, American Chemical Society. **g–h** Reprinted with permission from Ref. [32] Copyright 2018, American Chemical Society. **i–l** Reprinted with permission from Ref. [35] Copyright 2019, American Chemical Society

blue-emitting NCs with a PLQY close to 90% (Fig. 3i) [35]. The PL enhancement was ascribed to surface trap passivation of LHP (3-D) NCs during anion exchange, as depicted in Fig. 3i, j. The as-obtained NCs were utilized in blue-emitting (Fig. 3k) and security applications such as anti-counterfeiting inks. A trademark pattern of Lancôme was written on sulfuric paper using the NC ink. The pattern was only visible (because of the blue fluorescence of the NCs) under UV light. Wiping the Lancôme pattern's anticounterfeiting tags with cotton soaked in water resulted in the flower's disappearance, and the letters turned green under UV light. This helped authenticate the trademark [35]. Furthermore, Pradhan et al. reported that surface passivation with various metal and nonmetal chlorides and oleylammonium chloride salt results in a 40–50-fold enhancement in the emission intensity of $CsPbCl_3$ NCs [36]. This surface passivation also improved the phase stability of $CsPbCl_3$ NCs.

4 Organometal LHP NPLs

Various synthetic methods produce LHP NCs of various shapes and sizes in different dimensions with precise control [18, 37–40]. Quantum-confined LHP nanoplatelets (NPLs) are an alternative approach to obtaining bright blue emission. Conventional semiconducting quantum dots (QDs)

fall into this category [41]. The reduction of the size of the NCs in more than one dimension to less than twice of exciton Bohr radius results in quantum-confined particles. Both the absorption and PL maxima of the NCs undergo a blue shift upon quantum confinement. The color instability of blue-emitting $CsPb(Cl/Br)_3$ NCs, owing to the segregation of the halide ions, led to the exploration of these quantum-confined NPLs. Moreover, the blue-emitting LHP NCs were lagging behind the red- and green-emitting ones with low PLQYs, broad emission profiles, and poor colloidal stability. The excitonic Bohr radii of LHP materials are 2.5 nm ($CsPbCl_3$), 3.5 nm ($CsPbBr_3$), and 6 nm ($CsPbI_3$) [6, 42]. Therefore, the quantum confinement effect was achieved by decreasing the LHP thickness to a few monolayers, which in turn, led to a strong blue shift of the absorption onsets and the PL maxima [19, 20, 42, 43]. However, research on LHP NPLs is limited. One of the first reports on LHP NPLs was published by Sichert et al.which dealt with the quantum size effect in organometal halide NPLs [44]. Single-crystalline 2-D $(C_4H_9NH_3)_2PbBr_4$ nanosheets were fabricated on a substrate and detached subsequently [45]. Another early study reported the formation of $MAPbBr_3$ NPLs as a secondary product [46]. Since then, many efforts were made to obtain LHP NPLs with tunable thickness and tunable PL position by changing the halide ion from chloride to iodide [20, 42]. LHP NCs have been produced predominantly via solid-state crystallization method (produces LHP NPLs on a substrate) [45, 47, 48], chemical or physical exfoliation of bulk LHP [16, 49], hot-injection crystallization in a mixture of 1-octadecene, oleic acid, and oleylamine [5, 46, 50], and non-solvent crystallization from a polar solvent [40, 51]. However, all these methods produce colloidally stable NPLs except for solid-state crystallization.

On the other hand, bulk LHPs can be defined by ABX_3 (Fig. 4a), where A is a cation with a + 1 oxidation state, B is a metal ion with a + 2 oxidation state, and X is a halide ion with a − 1 oxidation state, LHP NPLs are described as $L_2[ABX_3]_{n-1}BX_4$. Here, L represents the ligand molecule, which is essential for NPL colloidal stability and growth control in one dimension. Substituting $n = 1$ in the NPL formula leads to a structure without A cations and $n = 2$ produces a complete perovskite unit cell, as shown in Fig. 4b, c, respectively. Therefore, the n-1 term represents the number of complete perovskite unit cells that fit within the thickness of the NPL. Precise thickness was attained for $n = 1$ and 2, whereas for $n = 3$, 4, etc., NPLs had varying thicknesses. Typical XRD patterns of $L_2[ABX_3]_{n-1}BX_4$ NPLs for n = 1 and 2 are shown in Fig. 4c. The XRD patterns of the NPL films exhibit additional and periodic diffraction peaks at the lower angles of the pattern, corresponding to the stacking of

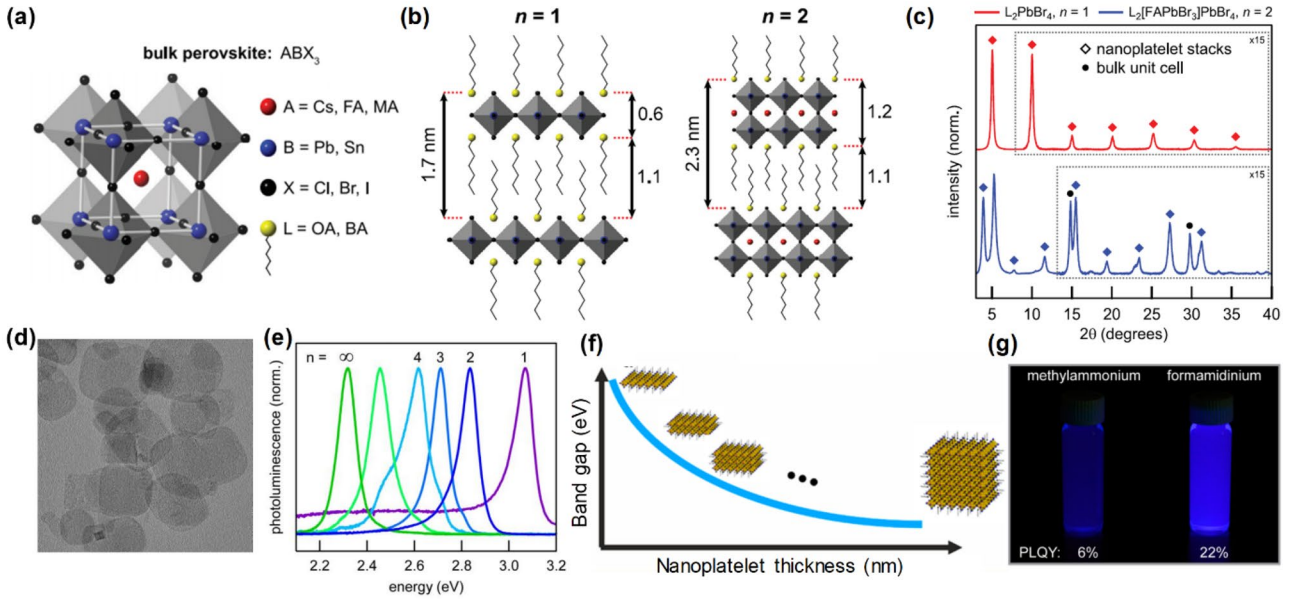

Fig. 4 Properties of organometal LHP NPLs. **a** Bulk perovskite unit cell (cube) and the possible elements/molecules for A, B, X, and L. **b** Representation of the NPL stacks and relevant distances. '*n*' and '*n*−1′ represent the layers of metal-halide octahedra and the number of complete unit cells incorporated in the NPL thickness, respectively. **c** XRD patterns for $n = 1$ (L_2PbBr_4) and $n = 2$ ($L_2[FAPbBr_3]PbBr_4$) NPLs showing periodic reflections from NPL stacks which form in the thin-film samples (diamond symbols). Black circles indicate reflections corresponding to the bulk perovskite unit cell **d** TEM image of $L_2[ABX_3]BX_4$ NPLs. **e** PL spectra of perovskite nanoplatelets of varying thicknesses. **f** The bandgap variation of the LHP NPLs as a function of platelet thickness. **g** Image of the $n = 2$ ($L_2[APbBr_3]PbBr_4$) sample under UV illumination, demonstrating the A-site cation dependency on PLQY. **a–e** and **g** Reprinted with permission from Ref. [51] Copyright 2016, American Chemical Society. **f** Reprinted with permission from Ref. [44] Copyright 2015, American Chemical Society

the NPLs. The diffraction peaks related to the NPL stacking are denoted by diamond symbols, as shown in Fig. 4c. NPLs with $n=1$ displayed intense stacking reflections, whereas the diffraction peaks related to the perovskite structure were feeble. Separation of the NPLs by embedding them with silica led to the clear appearance of reflections corresponding to the perovskite structure, verifying the formation of LHP NPLs. The stronger reflections that appeared from the NPL stacking were a consequence of the large lateral dimensions of the NPLs, which caused them to lie flat on the substrate and overlap with each other in a well-defined way when they were drop-casted as a film. However, the reflections corresponding to the perovskite structure are observed in NPLs where $n=2$, as shown in Fig. 4c. The XRD reflections related to NPL stacking were observed at regular intervals of 5.1° and 3.9° for $n=1$ and $n=2$ NPLs, respectively. The average spacing between the layers of NPLs obtained from these periodicities was 1.7 nm and 2.3 nm for $n=1$ and $n=2$ NPLs, respectively. The higher spacing in the case of $n=2$ NPLs is clear from its extensive perovskite structure compared to that of $n=1$ NPLs (Fig. 4b). Here, the metal-halide octahedron is typically 0.59–0.63 nm long, and the length of the ligands is between ~ 1 nm (octylammonium) and ~ 0.5 nm (butylammonium). Therefore, the spacing is expected to be almost unchanged regardless of the chemical composition of the NPLs.

The formation of the platelet structure was verified by transmission electron microscopy (TEM), as shown in Fig. 4d. The $L_2[ABX_3]BX_4$ NPLs have lateral dimensions of a few hundred nanometers [51]. AFM is also an effective tool for determining the NPL thickness. The thicknesses of the $(C_4H_9NH_3)_2PbBr_4$ sheets were measured using AFM [45]. The thicknesses of ~ 1.6 nm and ~ 3.4 nm were obtained for monolayer and double layer NPL sheets, respectively.

The emission of organometal LHP NPLs depends on their thicknesses, as shown in Fig. 4e. The PL maximum position is blue-shifted upon reducing the NPL thickness [44, 51]. The NPL thickness was controlled by tuning the ratio of organic cations [44]. The bandgap of the NPLs varies as a function of their thicknesses, owing to the quantum size effects, as shown in Fig. 4f. The optical properties of the NPLs also depend on the B-site cations, X-site ions, and A-site cations [51]. The possibility of deep-UV absorption in chlorides, violet/blue emission (bromides) to green/yellow emission (iodides) demonstrated the impact of halide ions on the electronic structure of the organometal LHP NPLs. Red-shifted absorption and PL spectra were observed upon replacing Pb with Sn. Increasing the A-site cation size from Cs to MA to FA gradually reduced their bandgap, and this size-dependent trend was also observed in the bulk materials [52, 53]. A variation in the A-site cation size affects the PLQY and FWHM of the NPLs. The PLQY of the blue-emitting $L_2[FAPbBr_3]PbBr_4$ NPLs was 22%, which was nearly four times higher than that of $L_2[MAPbBr_3]PbBr_4$ NPLs (PLQY = 6%), as shown in Fig. 4g. Therefore, FA was found to be an excellent A-site cation with better optical features such as high PLQY and narrow FWHM.

5 All-inorganic $CsPbBr_3$ LHP NPLs

The quantum confinement effect observed in the 2-D $L_2[ABX_3]_{n-1}BX_4$ NPLs arises by incorporating organic molecules in between the perovskite unit cells. Efforts have been made to synthesize $CsPbX_3$ NPLs [20, 42, 43, 54]. The reprecipitation method, which involves the precipitation of NPLs by adding polar solvents such as acetone to a toluene solution containing Pb, Cs, and halide precursors, was employed for producing $CsPbX_3$ NPLs [20, 42]. However, for synthesizing $CsPbBr_3$ NPLs, a specific Cs/Pb ratio (depending upon NPL thickness) was injected into a toluene-$PbBr_2$-capping ligand solution at room temperature. The $CsPbBr_3$ NPLs crystallized when excess acetone was added to the above reaction mixture, as shown in Fig. 5a. The thickness of the NPLs was controlled by regulating the molar ratio of the precursors during synthesis (Fig. 5b). NPLs as thin as a monolayer were obtained via this method. The resultant NPL solutions exhibited a clear difference in their emission color (under UV light), with a gradual change from blue to green as a function of the Cs/Pb ratio (Fig. 5b). This emission tuning was attributed to quantum confinement effects, and similar effects were observed in the case of organometal LHP NPLs (i.e., 2-D $L_2[ABX_3]_{n-1}BX_4$ NPLs).

The formation of blue-emitting $CsPbBr_3$ NPLs was investigated using annular dark-field-scanning transmission electron microscopy (ADF–STEM), as shown in Fig. 5c–e. Thicknesses measured from the ADF–STEM images were ~ 1.2 nm, ~ 2.0 nm, and ~ 2.9 nm for 2 (2-D), 3 (quasi 2-D), and 5 (quasi 2-D) monolayered NPLs, respectively. These values are close to the predicted values, based on the thickness of a single corner-shared $[PbBr_6]^{4-}$ octahedra, which is 0.6 nm [55]. The NPL formation was further confirmed by XRD [20, 42]. Figure 5f shows the absorption and PL spectra of the NPLs as a function of their thicknesses. As discussed above, both the PL and the absorption maxima were blue-shifted with decreasing NPL thickness. It is also clear from the absorption spectra that the excitonic absorption feature of the blue-emitting NPLs is narrow compared to the broad absorption feature of the nanocubes (green-emitting). This further suggests that the size (thickness) of the NPLs falls into the Bohr exciton radius regime. The exciton binding energy increased as the NPL thickness was reduced, and a value of 280 meV was obtained for the two monolayered $CsPbBr_3$ NPLs [20]. This is almost nine times the value for the green-emitting nanocubes (30 meV). Here,

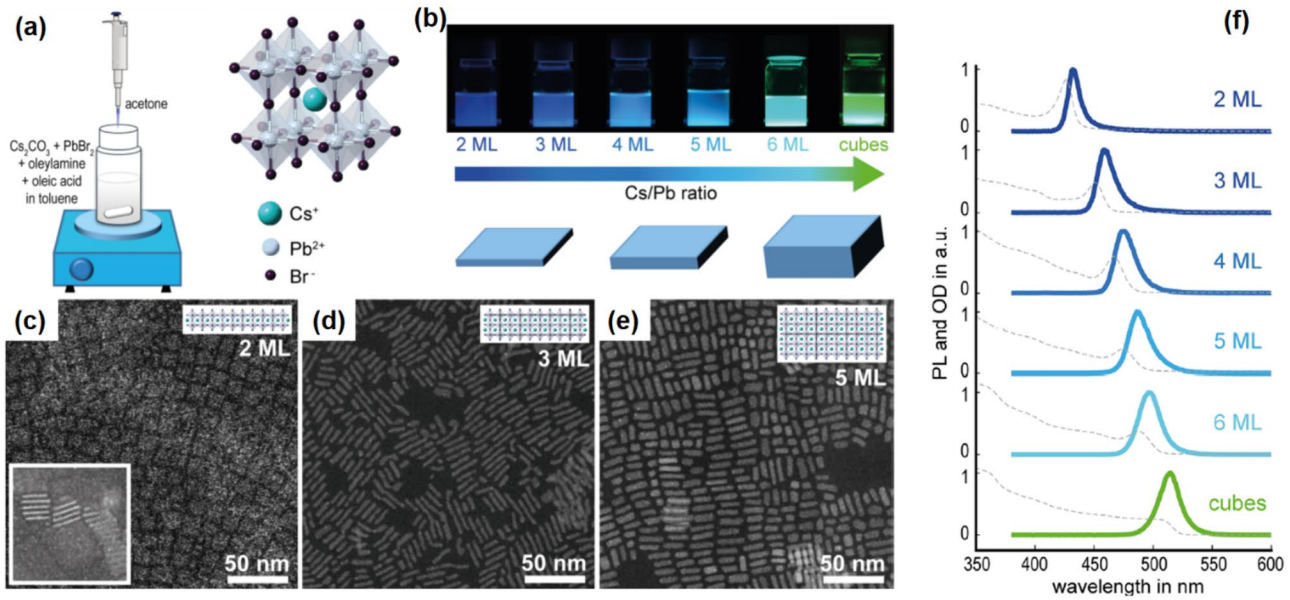

Fig. 5 **a** The synthesis of $CsPbBr_3$ NPLs via reprecipitation approach. **b** Photographs of colloidal NPL dispersions with varying precursor ratios under UV light. **c–e** ADF-STEM images of 2, 3, and 5 monolayered NPLs. **f** Comparison of PL (solid lines) and absorption (dashed lines) spectra of NPL colloids of varying NPL thickness with those of weakly confined nanocubes. Reprinted with permission from Ref. [20] Copyright 2018, American Chemical Society

the extent of the blue shift in the optical spectra of the NPLs would be large for higher exciton binding energies.

Although $CsPbBr_3$ NPLs with uniform thickness and narrow PL were synthesized, very low PLQYs (< 10%) were found for the thinner NPLs (2 and 3 monolayers) in the initial reports [42]. Such low PLQY values were attributed to the trapping of photogenerated charge carriers by the surface traps and the high surface-to-volume ratios of the 2-D nanostructures [20]. A few pathways were created to improve their PL intensities. Post-synthetic treatment of the NPLs with $PbBr_2$ led to a drastic increase in their PLQYs, without affecting their PL maximum, as shown in Fig. 6a. The PLQY increased from < 10% to 50–60% for 2 and 3 monolayer NPLs. Treatment with other agents such as $SnBr_2$ and KBr also led to a slight improvement, unlike $PbBr_2$, which affected the PLQYs. Furthermore, elemental analysis revealed that excess Pb and Br in the $PbBr_2$-treated NPLs compared to the untreated ones. Therefore, both Pb and Br surface trap states were eliminated upon $PbBr_2$-treatment, as depicted in the inset of Fig. 6a. Furthermore, PL enhancement was maximum for the thinnest NPLs, as shown in Fig. 6b. This study showed that surface passivation was crucial for obtaining luminescent LHP NPLs, and the removal of additional recombination (non-radiative) pathways was confirmed via TrPL spectroscopy (Fig. 6c). Furthermore, the in situ passivation of $PbBr_6^{4-}$ octahedra produced blue-emitting $CsPbBr_3$ NPLs with narrow emission and a PLQY of 96% [56]. The utilization of the only $PbBr_2$ during the NPL synthesis imparts a low PLQY, owing to the formation of bromide vacancies as the coordinate solvent or ligands compete with the halide ions to bind with the lead bromide octahedra. Consequently, employing excess bromide ions (by introducing HBr) during the NPL synthesis averted the vacancy formation and produced bright emitting NPLs, as demonstrated in Fig. 6d. This is one of the highest PLQY values reported for blue-emitting LHP NCs to date (Fig. 6e). Furthermore, 2-D LHP NPLs exhibit structural instability. Unprotected LHP NPLs agglomerate in either solvent or film form and lose their emission properties. For instance, blue-emitting $CsPbBr_3$ NPLs in ambient atmosphere gradually converted into green-emitting $CsPbBr_3$ nanocubes (Fig. 6f, g) [42, 57]. In some cases, the conversion took place within a few hours after the synthesis [58]. The high surface energy associated with the 2-D structures induced the coalescence of NPLs. Similar to the case of 3-D $CsPbX_3$ NCs, doping a smaller B-site cation such as Cu^{2+} into $CsPbBr_3$ NPLs improved their stability (Fig. 6h) [57]. The Cu^{2+}-doped NPLs exhibited improved ambient stabilities and resistance photodegradation. The improved stability observed in Cu^{2+}-doped NPLs was ascribed to the reduced surface energy of the NPLs aided by higher lead bromide octahedral rotation upon doping. In another report, surface passivation with $PbBr_2$ resulted in improvement in PL QY and photostability of blue-emitting NPLs (Fig. 6i) [20].

Quantum confinement was shown to be achieved in $CsPbBr_3$ by controlling the crystal size via thermodynamic equilibrium [59]. Wang et al. demonstrated that amino acids as chelating ligands improve the blue emission intensity of

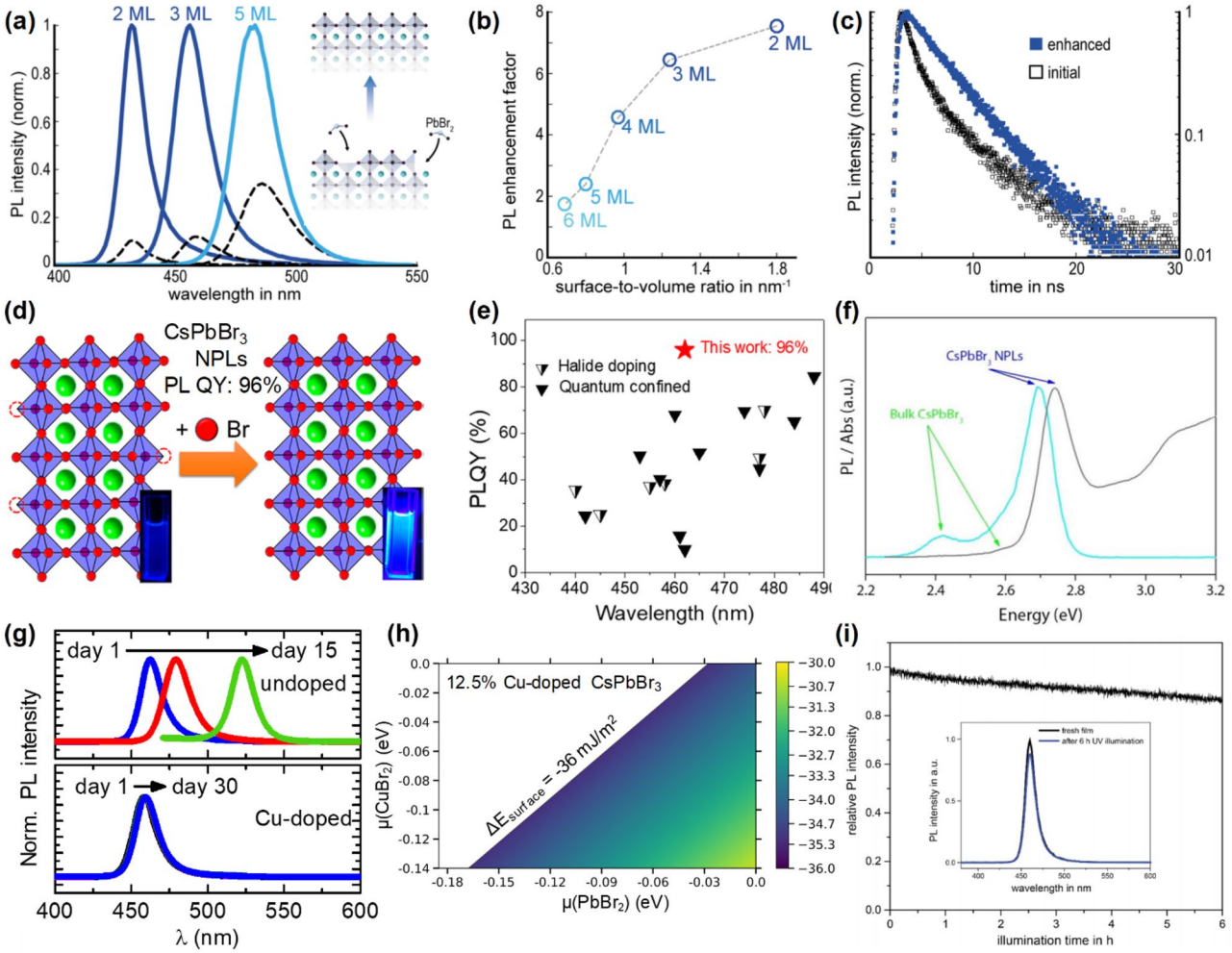

Fig. 6 Stability and PLQY enhancement of NPLs. **a** PL spectra of untreated $PbBr_2$-treated $CsPbBr_3$ NPL colloidal dispersions. Inset depicts the surface repairing process. **b** PL enhancement factor as a function of the surface-to-volume ratio of the NPLs. **c** TrPL spectra of a three-monolayer NPL dispersion before and after $PbBr_2$ treatment (enhancement). **d** Illustration of removal of Br^- vacancies in $PbBr_6^{4-}$ octahedra of $CsPbBr_3$ NPLs using HBr solution. **e** Comparison of the PLQY of Br-vacancy passivated $CsPbBr_3$ NPLs with other inorganic halide perovskite NCs. **f** PL spectra of fresh and 1-week-old 5-monolayer $CsPbBr_3$ NPLs in air. **g** Normalized PL spectra of undoped and Cu^{2+}-doped $CsPbBr_3$ NPLs when stored in ambient conditions. **h** Contour plot for the difference in surface energies of the 12.5% Cu^{2+}-doped and undoped CsPbBr3 within the chemical potential bounds. **i** Photostability measurement of a $PbBr_2$-treated 3-monolayer $CsPbBr_3$ NPL film prepared by spin-coating. The PL spectra of the film obtained before and after this illumination are shown in the inset. **a**–**c** and **i** Reprinted with permission from Ref. [20] Copyright 2018, American Chemical Society. **d** and **e** Reprinted with permission from Ref. [56] Copyright 2018, American Chemical Society. **f** Reprinted with permission from Ref. [42] Copyright 2016, American Chemical Society. **g** and **h** Reprinted with permission from Ref. [57] Copyright 2020, Elsevier

$CsPbBr_3$ quantum wires (QWs) by passivating the surface traps and emission stability under both acid and base [60]. γ-aminobutyric acid-passivated $CsPbBr_3$ QWs produced spectrally stable blue LEDs with an EQE as high as 6.3%. Recently, Sargent and coworkers have achieved an EQE of 12.3% for $CsPbBr_3$ QD-based blue LEDs via a bipolar-shell resurfacing approach [61]. This is the highest EQE value reported for halide perovskite-based blue LEDs. Bipolar shells such as isopropyl ammonium bromide remove the surface Br^- vacancies, which are detrimental to both PL and EL properties of the LHP QDs. Blue-emitting, bipolar-shell resurface LHP QD films exhibited PL QY above 90% and improved charge carrier mobility, which, in turn, resulted in the 12.3% EQE observed for the LHP-based blue LEDs [61].

So far, we have discussed the efforts to improve the structural and emission properties of blue-emitting LHP NCs and NPLs. One of the primary goals of these materials with bright emission characteristics is to utilize them for light-emitting applications. Although these materials initially exhibited very low efficiencies relative to green- and red-emitting LHP devices [20, 62, 63], a few recent strategies have considerably improved their efficiencies [33, 64–66].

6 Current interest: lead-free perovskite-type structures

Despite possessing the characteristics suitable for commercial photovoltaics and LEDs, the toxic nature of lead prevents its application for the said purpose. Hailegnaw et al. explained the influence of rain on $MAPbI_3$ film in case of solar plant failure and found that the perovskite material was degraded [67]. This would lead to the dissolution of PbI_2 in water, and, in turn, release lead into the underground water resources in the order of 10^{-8} mol L^{-1}. Therefore, suitable lead alternatives, such as tin, antimony, germanium, copper, or bismuth, should be employed. Perovskites based on these elements have exhibited promising blue emission [68–73]. In 2016, Leng et al. replaced Pb^{2+} ions with isoelectronic Bi^{3+} ions and synthesized $MA_3Bi_2Br_9$ perovskite-related QDs with an average diameter of 3 nm. $MA_3Bi_2Br_9$ QDs exhibited an emission maximum at approximately 430 nm (FWHM = 62 nm) and a PLQY of 12% [68]. The structure of the QDs is different from that of the conventional cubic phase perovskite. Although $MA_3Bi_2Br_9$ was not strongly blue-luminescent, halide passivation improved its emission intensity, as shown in Fig. 7a. The optimized chloride ion concentration boosted the blue PLQY to 54% (Fig. 7b). The chloride ions were mainly located on the QD surface and passivated the surface defects, owing to the mismatch in the crystal structures of $MA_3Bi_2Br_9$ and $MA_3Bi_2Cl_9$ [74]. Furthermore, $FA_3Bi_2Br_9$ QDs synthesized via a ligand-assisted process exhibited a PLQY of 52% at 437 nm, owing to the low defect density [70]. These QDs also displayed good air- and polar solvent stability. Blue-emitting $Cs_3Bi_2Br_9$ QDs displayed PL enhancement upon exposure to water owing to the hydrolysis product BiOBr, which acted as the surface passivation layer [75].

Sn^{2+} is a suitable replacement for Pb^{2+} in the LHP structure. Nevertheless, emission-tunable $CsSnX_3$ NCs were synthesized via hot-injection, as shown in Fig. 7c, d. However, they exhibited poor structural stability due to the oxidation of Sn^{2+} to Sn^{4+} [76]. This led to the deterioration of their optical properties. Sn^{4+} is stable against oxidation unlike Sn^{2+}. Therefore, environmentally stable and non-toxic Cs_2SnI_6 NCs with different shapes were synthesized

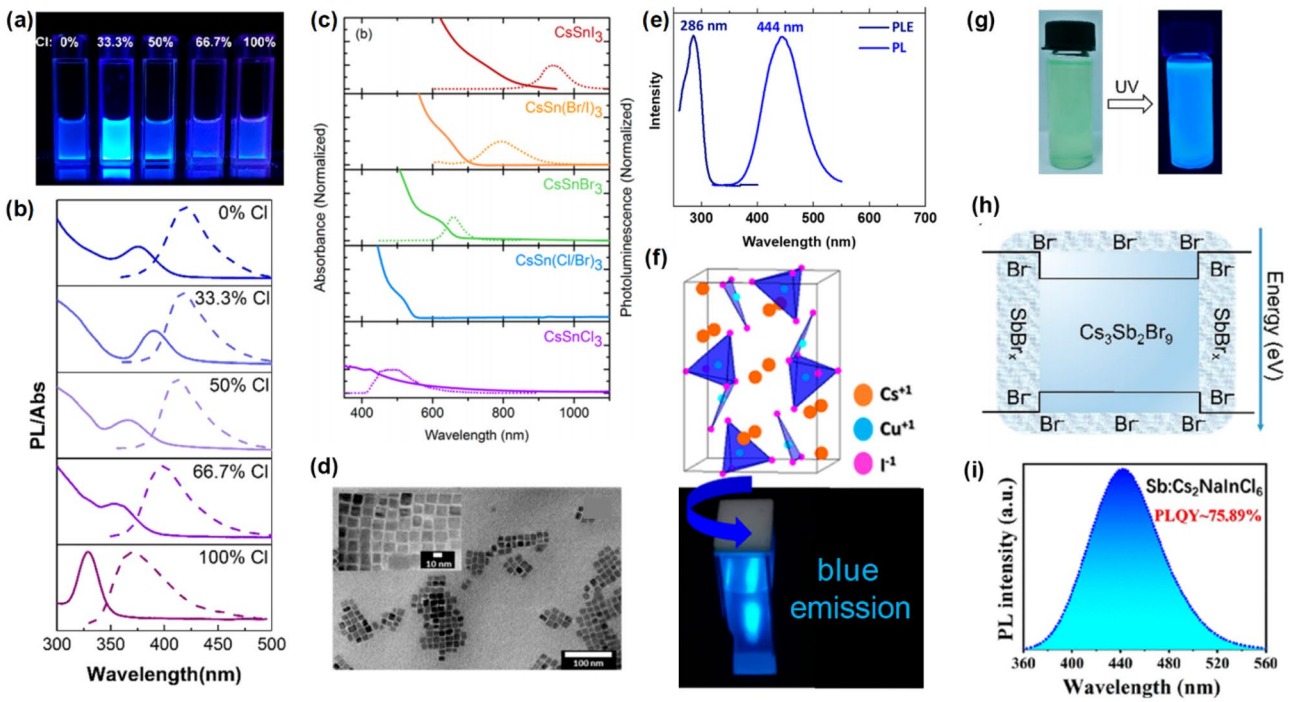

Fig. 7 **a** Photographs of $MA_3Bi_2(Cl, Br)_9$ QD solutions synthesized with different contents of Cl under a 325 nm UV lamp excitation and **b** displays the corresponding PL spectra. Reprinted with permission from Ref. [74] Copyright 2018, American Chemical Society. **c** Absorbance and steady-state PL of $CsSnX_3$ NCs. **d** TEM image of $CsSnX_3$ NCs. Reprinted with permission from Ref. [76] Copyright 2016, American Chemical Society. **e** PL excitation and emission spectra of $Cs_3Cu_2I_5$ NCs in hexane. **f** The crystal structure of $Cs_3Cu_2I_5$ and the NC solution under 365 nm light. Reprinted with permission from Ref. [78] Copyright 2019, American Chemical Society. **g** Typical optical images of a colloidal $Cs_3Sb_2Br_9$ NC solution with and without 365 nm UV light excitation and **h** proposed band structure diagram. Reprinted with permission from Ref. [73] Copyright 2017, American Chemical Society. **i** PL spectra of 10% Sb^{3+}:$Cs_2NaInCl_6$. Reprinted with permission from Ref. [79] Copyright 2020, American Chemical Society

Table 1 Representative strategies for enhancing blue emission intensity of LHPs

Composition	Improvement strategy	PL QY (%)	References
$CsPb(Cl,Br)_3$ NCs	Engineering the local order of the host lattice and trap state removal by Ni^{2+} doping	93	[25]
$CsPb(Cl,Br)_3$ NCs	Post-synthetic Cd^{2+} treatment/doping	98	[27]
$CsPbCl_3$ and $CsPb(Cl/Br)_3$ NCs	Suppression of unfavorable octahedral distortion and passivation of halide vacancies by $CuCl_2$ addition during synthesis	60–98	[29]
$CsPbCl_3$ NCs	Dual-surface passivation with Y^{3+} and Cl^- ions	60	[32]
$CsPbCl_3$ NCs	Removal of surface traps via anion exchange with Cs_4PbCl_6 NCs	90	[35]
$L_2[APbBr_3]PbBr_4$	Replacing methlammonium with formamidinium (A-site cation)	22	[51]
$CsPbBr_3$ NPLs	Surface trap removal by post-synthetic $PbBr_2$ treatment	50–73	[20]
$CsPbBr_3$ NPLs	Suppression of surface Br^- trap formation by introducing excess Br^- ions during synthesis	96	[56]
$Cs_2NaInCl_6$	Breaking of parity-forbidden transition rule by Sb^{3+} doping	75	[79]

by a hot-injection approach. They demonstrated a high hole mobility (> 20 $cm^2/(Vs)$) under ambient conditions but poor luminescence efficiencies [77]. However, bismuth doping led to the appearance of strong blue luminescence in lead-free Cs_2SnCl_6. The non-luminescent Cs_2SnCl_6 exhibited a broad emission with a maximum at 455 nm and a PLQY of nearly 80% upon doping. DFT calculations suggested that the $[Bi_{Sn} + V_{Cl}]$ defect complex was responsible for the observed blue emission [71]. The Cs_2SnCl_6:Bi also displayed strong resistance towards water degradation owing to the formation of BiOCl passivation layer. Cs_2SnCl_6:Bi was used as a blue-emissive phosphor in white LED construction.

Zero-dimensional Cu(I)-based $Cs_3Cu_2I_5$ was proposed as a novel lead-free and blue-luminescent material. It exhibited good ambient stability and a high PLQY of 90% [72, 80] as the bulk crystals, and 35% [78] in the nano form, as shown in Fig. 7e. The high luminescence and large exciton binding energy of 492 meV originated from its 0-D electronic structure, wherein the Cu-I photoactive sites are separated by Cs ions, as shown in Fig. 7f. Excited-state structural reorganization is the proposed luminescence mechanism. In a recent study, deep-blue LEDs with a high operational lifetime and an external quantum efficiency of ~ 1.12% based on these 0-D $Cs_3Cu_2I_5$ NCs were fabricated, and their efficiencies were comparable with those of the best-performing LHP-based blue LEDs [81]. Furthermore, Cs_2CuX_4 QDs exhibited tunable emission maxima from 385 to 468 nm upon changing the halide from chloride to bromide to iodide [82]. The PLQY values for Cs_2CuCl_4 and Cs_2CuBr_4 were ~ 52% and ~ 35%, respectively. The substitution of all the Pb^{2+} ions in $CsPbBr_3$ with Eu^{2+} ions produced $CsEuBr_3$ NCs with a narrow (FWHM = 30 nm) blue emission of 39% PLQY [83]. Furthermore, lead-free all-inorganic $Cs_3Sb_2Br_9$ QDs exhibited strong blue luminescence (emission maximum at 410 nm) with a PLQY of 46% (Fig. 7g) [73]. The high PLQY was a consequence of their high exciton binding energy. $Cs_3Sb_2Br_9$ QDs exhibited a quantum well structure, as shown in Fig. 7h. Recently, double perovskite structures of $Cs_2AgInCl_6$ and $Cs_2NaInCl_6$ have been exploited to attain interesting optical properties [84, 85]. The PLQY of the undoped ones is undetectable owing to the parity-forbidden transitions, although they exhibit a direct bandgap. Nevertheless, doping with trivalent ions such as Sb^{3+} produced blue-emitting $Cs_2NaInCl_6$ with a PLQY of ~ 75% [79]. The doping broke the parity-forbidden transition rule and also modified the density of states, thereby producing strong self-trapped exciton (STE) blue emission.

7 Summary and outlook

This review has summarized various approaches for producing blue-emitting LHP NCs and the different strategies for improving their PLQYs, as shown in Table 1. Furthermore, we have covered various aspects concerning the structure and optical properties of 2-D organometal and all-inorganic LHPs. In the last section, we introduced various lead-free perovskite-like systems that may interest material chemists and engineers. Although the PLQYs of blue-emitting and sky-blue-emitting LHP NCs reached near unity values, their EL efficiencies were very low when compared to those of the red- and green-emitting LHP NC-based devices. The presence of an inherent higher defect density and, importantly, the defects formed upon the loss of the capping ligands during film formation were detrimental to higher EL intensities in blue-emitting LHP NCs. Using capping ligands that bind strongly to the LHP NC surface might solve this issue [86]. Furthermore, doping of smaller cations into the B-site of the NCs would improve the stability and performance of the EL devices. The shift in the emission position of the blue-emitting $CsPb(Cl/Br)_3$ NCs under the electric field needs in-depth understanding. The reduction in the dimensions of the NCs led to the production of blue emission with a single halide, and the 2-D LHP NPLs were thought to be the replacement for the $CsPb(Cl/Br)_3$ NCs. However, the 2-D NPLs suffer from agglomeration-induced emission color instability

in the film form. The EQE of blue-emitting 2-D NPLs was very low owing to the PLQY loss at the interface [64]. Recognizing and eliminating the interfacial losses can enhance their EQE values. Last but not least, blue emitting lead-free perovskite NCs or bulk have been produced via B-site modification. Although they achieved very high PLQYs, their EL properties remained unexplored. Moreover, the low dimensionality in their crystal structure, which means decoupled emission centers, is also an enormous concern for fabricating efficient EL-based optoelectronic devices. For instance, a maximum EQE of only ~ 1% was achieved for the $Cs_3Cu_2I_5$ NCs. They exhibit broadband emission owing to the origin of the STE phenomenon. Therefore, the quest for synthesizing new lead-free materials continues. A combined theoretical and experimental approach can be employed to obtain new lead-free materials with narrow emission characteristics and of 3D structural dimensions. For instance, out of 90 hypothetical 2-D double perovskites possible, five new compositions such as $Cs_4CdSb_2Cl_{12}$ and $Cs_4MnBi_2Cl_{12}$, with a general formula of $A_4M^{II}M^{III}{}_2X_{12}$ were experimentally synthesized, and some of them exhibited promising properties for use in optoelectronics applications [87]. Future studies can involve the exploration and synthesis of more materials with probable metals and halides using this technique, followed by studying their properties and possible applications.

Acknowledgements This work was supported by the Materials Innovation Project (2020M3H4A3081792) funded by the National Research Foundation of Korea and the Technology Innovation Program (KEIT-20010737) funded by the Ministry of Trade, Industry & Energy (MOTIE, Korea).

References

1. N. Zhang, Y. Fan, K. Wang, Z. Gu, Y. Wang, L. Ge, S. Xiao, Q. Song, All-optical control of lead halide perovskite microlasers. Nat. commun. **10**(1), 1–7 (2019)
2. Y.C. Kim, K.H. Kim, D.-Y. Son, D.-N. Jeong, J.-Y. Seo, Y.S. Choi, I.T. Han, S.Y. Lee, N.-G. Park, Printable organometallic perovskite enables large-area, low-dose X-ray imaging. Nature **550**(7674), 87–91 (2017)
3. Q. Chen, J. Wu, X. Ou, B. Huang, J. Almutlaq, A.A. Zhumekenov, X. Guan, S. Han, L. Liang, Z. Yi, All-inorganic perovskite nanocrystal scintillators. Nature **561**(7721), 88–93 (2018)
4. J. Feng, C. Gong, H. Gao, W. Wen, Y. Gong, X. Jiang, B. Zhang, Y. Wu, Y. Wu, H. Fu, Single-crystalline layered metal-halide perovskite nanowires for ultrasensitive photodetectors. Nat. Electron. **1**(7), 404–410 (2018)
5. L.C. Schmidt, A. Pertegás, S. González-Carrero, O. Malinkiewicz, S. Agouram, G. Minguez Espallargas, H.J. Bolink, R.E. Galian, J. Pérez-Prieto, Nontemplate synthesis of CH3NH3PbBr 3 perovskite nanoparticles. J. Am. Chem. Soc. **136**(3), 850–853 (2014)
6. L. Protesescu, S. Yakunin, M.I. Bodnarchuk, F. Krieg, R. Caputo, C.H. Hendon, R.X. Yang, A. Walsh, M.V. Kovalenko, Nanocrystals of cesium lead halide perovskites ($CsPbX_3$, X= Cl, Br, and I): novel optoelectronic materials showing bright emission with wide color gamut. Nano Lett. **15**(6), 3692–3696 (2015)
7. R.E. Brandt, J.R. Poindexter, P. Gorai, R.C. Kurchin, R.L. Hoye, L. Nienhaus, M.W. Wilson, J.A. Polizzotti, R. Sereika, R. Žaltauskas, Searching for "defect-tolerant" photovoltaic materials: combined theoretical and experimental screening. Chem. Mater. **29**(11), 4667–4674 (2017)
8. A. Buin, P. Pietsch, J. Xu, O. Voznyy, A.H. Ip, R. Comin, E.H. Sargent, Materials processing routes to trap-free halide perovskites. Nano Lett. **14**(11), 6281–6286 (2014)
9. M.A. Becker, R. Vaxenburg, G. Nedelcu, P.C. Sercel, A. Shabaev, M.J. Mehl, J.G. Michopoulos, S.G. Lambrakos, N. Bernstein, J.L. Lyons, Bright triplet excitons in caesium lead halide perovskites. Nature **553**(7687), 189–193 (2018)
10. Y. Shirasaki, G.J. Supran, M.G. Bawendi, V. Bulović, Emergence of colloidal quantum-dot light-emitting technologies. Nat. Photonics **7**(1), 13 (2013)
11. Y. Shynkarenko, M.I. Bodnarchuk, C. Bernasconi, Y. Berezovska, V. Verteletskyi, S.T. Ochsenbein, M.V. Kovalenko, Direct synthesis of quaternary alkylammonium-capped perovskite nanocrystals for efficient blue and green light-emitting diodes. ACS Energy Lett. **4**(11), 2703–2711 (2019)
12. J. Song, J. Li, L. Xu, J. Li, F. Zhang, B. Han, Q. Shan, H. Zeng, Room-temperature triple-ligand surface engineering synergistically boosts ink stability, recombination dynamics, and charge injection toward EQE-11.6% perovskite QLEDs. Adv. Mater. **30**(30), 1800764 (2018)
13. X. Shen, Y. Zhang, S.V. Kershaw, T. Li, C. Wang, X. Zhang, W. Wang, D. Li, Y. Wang, M. Lu, Zn-alloyed $CsPbI_3$ nanocrystals for highly efficient perovskite light-emitting devices. Nano Lett. **19**(3), 1552–1559 (2019)
14. G. Almeida, L. Goldoni, Q. Akkerman, Z. Dang, A.H. Khan, S. Marras, I. Moreels, L. Manna, Role of acid–base equilibria in the size, shape, and phase control of cesium lead bromide nanocrystals. ACS Nano **12**(2), 1704–1711 (2018)
15. A. Pan, B. He, X. Fan, Z. Liu, J.J. Urban, A.P. Alivisatos, L. He, Y. Liu, Insight into the ligand-mediated synthesis of colloidal $CsPbBr_3$ perovskite nanocrystals: the role of organic acid, base, and cesium precursors. ACS Nano **10**(8), 7943–7954 (2016)
16. V.A. Hintermayr, A.F. Richter, F. Ehrat, M. Döblinger, W. Vanderlinden, J.A. Sichert, Y. Tong, L. Polavarapu, J. Feldmann, A.S. Urban, Tuning the optical properties of perovskite nanoplatelets through composition and thickness by ligand-assisted exfoliation. Adv. Mater. **28**(43), 9478–9485 (2016)
17. L. Protesescu, S. Yakunin, O. Nazarenko, D.N. Dirin, M.V. Kovalenko, Low-cost synthesis of highly luminescent colloidal lead halide perovskite nanocrystals by wet ball milling. ACS Appl. Nano Mater **1**(3), 1300–1308 (2018)
18. F. Zhang, H. Zhong, C. Chen, X.-G. Wu, X. Hu, H. Huang, J. Han, B. Zou, Y. Dong, Brightly luminescent and color-tunable colloidal $CH_3NH_3PbX_3$ (X= Br, I, Cl) quantum dots: potential alternatives for display technology. ACS Nano **9**(4), 4533–4542 (2015)
19. I. Levchuk, A. Osvet, X. Tang, M. Brandl, J.D. Perea, F. Hoegl, G.J. Matt, R. Hock, M. Batentschuk, C.J. Brabec, Brightly luminescent and color-tunable formamidinium lead halide perovskite $FAPbX_3$ (X= Cl, Br, I) colloidal nanocrystals. Nano Lett. **17**(5), 2765–2770 (2017)
20. B.J. Bohn, Y. Tong, M. Gramlich, M.L. Lai, M. Döblinger, K. Wang, R.L. Hoye, P. Müller-Buschbaum, S.D. Stranks, A.S. Urban, Boosting tunable blue luminescence of halide perovskite nanoplatelets through postsynthetic surface trap repair. Nano Lett. **18**(8), 5231–5238 (2018)
21. M. Imran, V. Caligiuri, M. Wang, L. Goldoni, M. Prato, R. Krahne, L. De Trizio, L. Manna, Benzoyl halides as alternative precursors for the colloidal synthesis of lead-based halide perovskite nanocrystals. J. Am. Chem. Soc. **140**(7), 2656–2664 (2018)
22. G. Nedelcu, L. Protesescu, S. Yakunin, M.I. Bodnarchuk, M.J. Grotevent, M.V. Kovalenko, Fast anion-exchange in highly

luminescent nanocrystals of cesium lead halide perovskites ($CsPbX_3$, X= Cl, Br, I). Nano Lett. **15**(8), 5635–5640 (2015)
23. M. Liu, G. Zhong, Y. Yin, J. Miao, K. Li, C. Wang, X. Xu, C. Shen, H. Meng, Aluminum-doped cesium lead bromide perovskite nanocrystals with stable blue photoluminescence used for display backlight. Adv. Sci. **4**(11), 1700335 (2017)
24. W. Van der Stam, J.J. Geuchies, T. Altantzis, K.H. Van Den Bos, J.D. Meeldijk, S. Van Aert, S. Bals, D. Vanmaekelbergh, C. de Mello Donega, Highly emissive divalent-ion-doped colloidal CsPb1–xMxBr 3 perovskite nanocrystals through cation exchange. J. Am. Chem. Soc. **139**(11), 4087–4097 (2017)
25. Z.-J. Yong, S.-Q. Guo, J.-P. Ma, J.-Y. Zhang, Z.-Y. Li, Y.-M. Chen, B.-B. Zhang, Y. Zhou, J. Shu, J.-L. Gu, Doping-enhanced short-range order of perovskite nanocrystals for near-unity violet luminescence quantum yield. J. Am. Chem. Soc. **140**(31), 9942–9951 (2018)
26. S. Thawarkar, P.J.S. Rana, R. Narayan, S.P. Singh, Ni-doped $CsPbBr_3$ perovskite: synthesis of highly stable nanocubes. Langmuir **35**(52), 17150–17155 (2019)
27. N. Mondal, A. De, A. Samanta, Achieving near-unity photoluminescence efficiency for blue-violet-emitting perovskite nanocrystals. ACS Energy Lett. **4**(1), 32–39 (2018)
28. D. Parobek, B.J. Roman, Y. Dong, H. Jin, E. Lee, M. Sheldon, D.H. Son, Exciton-to-dopant energy transfer in Mn-doped cesium lead halide perovskite nanocrystals. Nano Lett. **16**(12), 7376–7380 (2016)
29. A. De, S. Das, N. Mondal, A. Samanta, Highly luminescent violet-and blue-emitting stable perovskite nanocrystals. ACS Mater. Lett. **1**(1), 116–122 (2019)
30. C. Bi, S. Wang, Q. Li, S.V. Kershaw, J. Tian, A.L. Rogach, Thermally stable copper (II)-Doped cesium lead halide perovskite quantum dots with strong blue emission. J. Phys. Chem. Lett. **10**(5), 943–952 (2019)
31. Y.-C. Chen, H.-L. Chou, J.-C. Lin, Y.-C. Lee, C.-W. Pao, J.-L. Chen, C.-C. Chang, R.-Y. Chi, T.-R. Kuo, C.-W. Lu, Enhanced luminescence and stability of cesium lead halide perovskite $CsPbX_3$ nanocrystals by Cu^{2+}-assisted anion exchange reactions. J. Phys. Chem. C **123**(4), 2353–2360 (2019)
32. G.H. Ahmed, J.K. El-Demellawi, J. Yin, J. Pan, D.B. Velusamy, M.N. Hedhili, E. Alarousu, O.M. Bakr, H.N. Alshareef, O.F. Mohammed, Giant photoluminescence enhancement in $CsPbCl_3$ perovskite nanocrystals by simultaneous dual-surface passivation. ACS Energy Lett. **3**(10), 2301–2307 (2018)
33. X. Zheng, S. Yuan, J. Liu, J. Yin, F. Yuan, W.-S. Shen, K. Yao, M. Wei, C. Zhou, and K. Song, Chlorine vacancy passivation in mixed-halide perovskite quantum dots by organic pseudohalides enables efficient Rec. 2020 blue light-emitting diodes. *ACS Energy Lett.* (2020).
34. H. Shao, X. Bai, G. Pan, H. Cui, J. Zhu, Y. Zhai, J. Liu, B. Dong, L. Xu, H. Song, Highly efficient and stable blue-emitting CsPbBr 3@ SiO2 nanospheres through low temperature synthesis for nanoprinting and WLED. Nanotechnology **29**(28), 285706 (2018)
35. C. Sun, Z. Gao, H. Liu, L. Wang, Y. Deng, P. Li, H. Li, Z.-H. Zhang, C. Fan, W. Bi, One stone, two birds: high-efficiency blue-emitting perovskite nanocrystals for LED and security ink applications. Chem. Mater. **31**(14), 5116–5123 (2019)
36. R.K. Behera, S. Das Adhikari, S.K. Dutta, A. Dutta, N. Pradhan, Blue-emitting $CsPbCl_3$ nanocrystals: impact of surface passivation for unprecedented enhancement and loss of optical emission. J. Phys. Chem. Lett. **9**(23), 6884–6891 (2018)
37. O. Vybornyi, S. Yakunin, M.V. Kovalenko, Polar-solvent-free colloidal synthesis of highly luminescent alkylammonium lead halide perovskite nanocrystals. Nanoscale **8**(12), 6278–6283 (2016)
38. M.B. Teunis, M.A. Johnson, B.B. Muhoberac, S. Seifert, R. Sardar, Programmable colloidal approach to hierarchical structures of methylammonium lead bromide perovskite nanocrystals with bright photoluminescent properties. Chem. Mater. **29**(8), 3526–3537 (2017)
39. Y. Zhang, M.I. Saidaminov, I. Dursun, H. Yang, B. Murali, E. Alarousu, E. Yengel, B.A. Alshankiti, O.M. Bakr, O.F. Mohammed, Zero-dimensional Cs_4PbBr_6 perovskite nanocrystals. J. Phys. Chem. Lett. **8**(5), 961–965 (2017)
40. S. Sun, D. Yuan, Y. Xu, A. Wang, Z. Deng, Ligand-mediated synthesis of shape-controlled cesium lead halide perovskite nanocrystals via reprecipitation process at room temperature. ACS Nano **10**(3), 3648–3657 (2016)
41. J.M. Pietryga, Y.-S. Park, J. Lim, A.F. Fidler, W.K. Bae, S. Brovelli, V.I. Klimov, Spectroscopic and device aspects of nanocrystal quantum dots. Chem. Rev. **116**(18), 10513–10622 (2016)
42. Q.A. Akkerman, S.G. Motti, A.R. Srimath Kandada, E. Mosconi, V. D'Innocenzo, G. Bertoni, S. Marras, B.A. Kamino, L. Miranda, F. De Angelis, Solution synthesis approach to colloidal cesium lead halide perovskite nanoplatelets with monolayer-level thickness control. J. Am. Chem. Soc. **138**(3), 1010–1016 (2016)
43. H. Huang, Y. Li, Y. Tong, E.P. Yao, M.W. Feil, A.F. Richter, M. Döblinger, A.L. Rogach, J. Feldmann, L. Polavarapu, Spontaneous crystallization of perovskite nanocrystals in nonpolar organic solvents: a versatile approach for their shape-controlled synthesis. Angew. Chem. Int. Ed. **58**(46), 16558–16562 (2019)
44. J.A. Sichert, Y. Tong, N. Mutz, M. Vollmer, S. Fischer, K.Z. Milowska, R. García Cortadella, B. Nickel, C. Cardenas-Daw, J.K. Stolarczyk, Quantum size effect in organometal halide perovskite nanoplatelets. Nano Lett. **15**(10), 6521–6527 (2015)
45. L. Dou, A.B. Wong, Y. Yu, M. Lai, N. Kornienko, S.W. Eaton, A. Fu, C.G. Bischak, J. Ma, T. Ding, Atomically thin two-dimensional organic-inorganic hybrid perovskites. Science **349**(6255), 1518–1521 (2015)
46. P. Tyagi, S.M. Arveson, W.A. Tisdale, Colloidal organohalide perovskite nanoplatelets exhibiting quantum confinement. J Phys. Chem. Lett. **6**(10), 1911–1916 (2015)
47. D.B. Mitzi, C. Feild, W. Harrison, A. Guloy, Conducting tin halides with a layered organic-based perovskite structure. Nature **369**(6480), 467–469 (1994)
48. J. Calabrese, N. Jones, R. Harlow, N. Herron, D. Thorn, Y. Wang, Preparation and characterization of layered lead halide compounds. J. Am. Chem. Soc. **113**(6), 2328–2330 (1991)
49. Y. Tong, E. Bladt, M.F. Aygüler, A. Manzi, K.Z. Milowska, V.A. Hintermayr, P. Docampo, S. Bals, A.S. Urban, L. Polavarapu, Highly luminescent cesium lead halide perovskite nanocrystals with tunable composition and thickness by ultrasonication. Angew. Chem. Int. Ed. **55**(44), 13887–13892 (2016)
50. Y. Bekenstein, B.A. Koscher, S.W. Eaton, P. Yang, A.P. Alivisatos, Highly luminescent colloidal nanoplates of perovskite cesium lead halide and their oriented assemblies. J. Am. Chem. Soc. **137**(51), 16008–16011 (2015)
51. M.C. Weidman, M. Seitz, S.D. Stranks, W.A. Tisdale, Highly tunable colloidal perovskite nanoplatelets through variable cation, metal, and halide composition. ACS Nano **10**(8), 7830–7839 (2016)
52. C.C. Stoumpos, M.G. Kanatzidis, The renaissance of halide perovskites and their evolution as emerging semiconductors. Acc. Chem. Res. **48**(10), 2791–2802 (2015)
53. G.E. Eperon, S.D. Stranks, C. Menelaou, M.B. Johnston, L.M. Herz, H.J. Snaith, Formamidinium lead trihalide: a broadly tunable perovskite for efficient planar heterojunction solar cells. Energy Environ. Sci. **7**(3), 982–988 (2014)
54. W.J. Mir, M. Jagadeeswararao, S. Das, A. Nag, Colloidal Mn-doped cesium lead halide perovskite nanoplatelets. ACS Energy Lett. **2**(3), 537–543 (2017)

55. L. Peng, A. Dutta, R. Xie, W. Yang, N. Pradhan, Dot–wire–platelet–cube: step growth and structural transformations in $CsPbBr_3$ perovskite nanocrystals. ACS Energy Lett. **3**(8), 2014–2020 (2018)
56. Y. Wu, C. Wei, X. Li, Y. Li, S. Qiu, W. Shen, B. Cai, Z. Sun, D. Yang, Z. Deng, In situ passivation of $PbBr_6^4$–octahedra toward blue luminescent $CsPbB_r3$ nanoplatelets with near 100% absolute quantum yield. ACS Energy Lett. **3**(9), 2030–2037 (2018)
57. G.K. Grandhi, H.M. Likhit, S.P. Ong, W.B. Im, Jahn–Teller distortion-driven robust blue-light-emitting perovskite nanoplatelets. Appl. Mater. Today **20**, 100668 (2020)
58. V.K. Ravi, A. Swarnkar, R. Chakraborty, A. Nag, Excellent green but less impressive blue luminescence from CsPbBr 3 perovskite nanocubes and nanoplatelets. Nanotechnology **27**(32), 325708 (2016)
59. Y. Dong, T. Qiao, D. Kim, D. Parobek, D. Rossi, D.H. Son, Precise control of quantum confinement in cesium lead halide perovskite quantum dots via thermodynamic equilibrium. Nano Lett. **18**(6), 3716–3722 (2018)
60. Y.-K. Wang, D. Ma, F. Yuan, K. Singh, J.M. Pina, A. Johnston, Y. Dong, C. Zhou, B. Chen, B. Sun, Chelating-agent-assisted control of CsPbBr 3 quantum well growth enables stable blue perovskite emitters. Nat. Commun. **11**(1), 1–7 (2020)
61. Y. Dong, Y.-K. Wang, F. Yuan, A. Johnston, Y. Liu, D. Ma, M.-J. Choi, B. Chen, M. Chekini, S.-W. Baek, Bipolar-shell resurfacing for blue LEDs based on strongly confined perovskite quantum dots. Nat. Nanotechnol. **15**(8), 668–674 (2020)
62. J. Song, J. Li, X. Li, L. Xu, Y. Dong, H. Zeng, Quantum dot light-emitting diodes based on inorganic perovskite cesium lead halides ($CsPbX_3$). Adv. Mater. **27**(44), 7162–7167 (2015)
63. G. Li, F.W.R. Rivarola, N.J. Davis, S. Bai, T.C. Jellicoe, F. de la Peña, S. Hou, C. Ducati, F. Gao, R.H. Friend, Highly efficient perovskite nanocrystal light-emitting diodes enabled by a universal crosslinking method. Adv. Mater. **28**(18), 3528–3534 (2016)
64. R.L. Hoye, M.-L. Lai, M. Anaya, Y. Tong, K. Gałkowski, T. Doherty, W. Li, T.N. Huq, S. Mackowski, L. Polavarapu, Identifying and reducing interfacial losses to enhance color-pure electroluminescence in blue-emitting perovskite nanoplatelet light-emitting diodes. ACS Energy Lett. **4**(5), 1181–1188 (2019)
65. M. Zhao, Y. Zhou, M.S. Molokeev, Q. Zhang, Q. Liu, Z. Xia, Discovery of new narrow-band phosphors with the UCr4C4-related type structure by alkali cation effect. Adv. Opt. Mater. **7**(6), 1801631 (2019)
66. S. Hou, M.K. Gangishetty, Q. Quan, D.N. Congreve, Efficient blue and white perovskite light-emitting diodes via manganese doping. Joule **2**(11), 2421–2433 (2018)
67. B. Hailegnaw, S. Kirmayer, E. Edri, G. Hodes, D. Cahen, Rain on methylammonium lead iodide based perovskites: possible environmental effects of perovskite solar cells. J. Phys. Chem. Lett. **6**(9), 1543–1547 (2015)
68. M. Leng, Z. Chen, Y. Yang, Z. Li, K. Zeng, K. Li, G. Niu, Y. He, Q. Zhou, J. Tang, Lead-free, blue emitting bismuth halide perovskite quantum dots. Angew. Chem. Int. Ed. **55**(48), 15012–15016 (2016)
69. B. Yang, J. Chen, F. Hong, X. Mao, K. Zheng, S. Yang, Y. Li, T. Pullerits, W. Deng, K. Han, Lead-free, air-stable all-inorganic cesium bismuth halide perovskite nanocrystals. Angew. Chem. Int. Ed. **56**(41), 12471–12475 (2017)
70. Y. Shen, J. Yin, B. Cai, Z. Wang, Y. Dong, X. Xu, and H. Zeng, Lead-free, stable, high-efficiency (52%) blue luminescent $FA_3Bi_2Br_9$ perovskite quantum dots. *Nanoscale Horiz.* (2020).
71. Z. Tan, J. Li, C. Zhang, Z. Li, Q. Hu, Z. Xiao, T. Kamiya, H. Hosono, G. Niu, E. Lifshitz, Highly efficient blue-emitting Bi-doped Cs2SnCl6 perovskite variant: photoluminescence induced by impurity doping. Adv. Func. Mater. **28**(29), 1801131 (2018)
72. T. Jun, K. Sim, S. Iimura, M. Sasase, H. Kamioka, J. Kim, H. Hosono, Lead-free highly efficient blue-emitting Cs3Cu2I5 with 0D electronic STRUCTURE. Adv. Mater. **30**(43), 1804547 (2018)
73. J. Zhang, Y. Yang, H. Deng, U. Farooq, X. Yang, J. Khan, J. Tang, H. Song, High quantum yield blue emission from lead-free inorganic antimony halide perovskite colloidal quantum dots. ACS Nano **11**(9), 9294–9302 (2017)
74. M. Leng, Y. Yang, Z. Chen, W. Gao, J. Zhang, G. Niu, D. Li, H. Song, J. Zhang, S. Jin, Surface passivation of bismuth-based perovskite variant quantum dots to achieve efficient blue emission. Nano Lett. **18**(9), 6076–6083 (2018)
75. M. Leng, Y. Yang, K. Zeng, Z. Chen, Z. Tan, S. Li, J. Li, B. Xu, D. Li, M.P. Hautzinger, All-inorganic bismuth-based perovskite quantum dots with bright blue photoluminescence and excellent stability. Adv. Func. Mater. **28**(1), 1704446 (2018)
76. T.C. Jellicoe, J.M. Richter, H.F. Glass, M. Tabachnyk, R. Brady, S.N.E. Dutton, A. Rao, R.H. Friend, D. Credgington, N.C. Greenham, Synthesis and optical properties of lead-free cesium tin halide perovskite nanocrystals. J. Am. Chem. Soc. **138**(9), 2941–2944 (2016)
77. A. Wang, X. Yan, M. Zhang, S. Sun, M. Yang, W. Shen, X. Pan, P. Wang, Z. Deng, Controlled synthesis of lead-free and stable perovskite derivative Cs2SnI6 nanocrystals via a facile hot-injection process. Chem. Mater. **28**(22), 8132–8140 (2016)
78. P. Vashishtha, G.V. Nutan, B.E. Griffith, Y. Fang, D. Giovanni, M. Jagadeeswararao, T.C. Sum, N. Mathews, S.G. Mhaisalkar, J.V. Hanna, Cesium copper iodide tailored nanoplates and nanorods for blue, yellow, and white emission. Chem. Mater. **31**(21), 9003–9011 (2019)
79. R. Zeng, L. Zhang, Y. Xue, B. Ke, Z. Zhao, D. Huang, Q. Wei, W. Zhou, and B. Zou, Highly Efficient Blue Emission from Self-Trapped Excitons in Stable Sb^{3+}-Doped $Cs_2NaInCl_6$ Double Perovskites. *J. Phys. Chem. Lett.* (2020).
80. F. Zhang, Z. Zhao, B. Chen, H. Zheng, L. Huang, Y. Liu, Y. Wang, and A. L. Rogach, Strongly emissive lead-free 0D $Cs_3Cu_2I_5$ perovskites synthesized by a room temperature solvent evaporation crystallization for down-conversion light-emitting devices and fluorescent inks. *Adv. Opt. Mater.* 1901723 (2020).
81. L. Wang, Z. Shi, Z. Ma, D. Yang, F. Zhang, X. Ji, M. Wang, X. Chen, G. Na, S. Chen, D. Wu, Y. Zhang, X. Li, L. Zhang, and C. Shan, Colloidal synthesis of ternary copper halides nanocrystals for high-efficiency deep-blue light-emitting diodes with a half-lifetime above 100 hours. *Nano Lett.* (2020).
82. P. Yang, G. Liu, B. Liu, X. Liu, Y. Lou, J. Chen, Y. Zhao, All-inorganic Cs_2CuX_4 (X= Cl, Br, and Br/I) perovskite quantum dots with blue-green luminescence. Chem. Commun. **54**(82), 11638–11641 (2018)
83. F. Alam, K.D. Wegner, S. Pouget, L. Amidani, K. Kvashnina, D. Aldakov, P. Reiss, Eu^{2+}: a suitable substituent for Pb^{2+} in $CsPbX_3$ perovskite nanocrystals? J. Chem. Phys. **151**(23), 231101 (2019)
84. J. Luo, X. Wang, S. Li, J. Liu, Y. Guo, G. Niu, L. Yao, Y. Fu, L. Gao, Q. Dong, Efficient and stable emission of warm-white light from lead-free halide double perovskites. Nature **563**(7732), 541–545 (2018)
85. A. Nag, Synthesis and luminescence of Mn-doped $Cs_2AgInCl_6$ double perovskites. Chem. Commun. **54**(41), 5205–5208 (2018)
86. J. Pan, Y. Shang, J. Yin, M. De Bastiani, W. Peng, I. Dursun, L. Sinatra, A.M. El-Zohry, M.N. Hedhili, A.-H. Emwas, O.F. Mohammed, Z. Ning, O.M. Bakr, Bidentate ligand-passivated $CsPbI_3$ perovskite nanocrystals for stable near-unity photoluminescence quantum yield and efficient red light-emitting diodes. J. Am. Chem. Soc. **140**(2), 562–565 (2018)
87. B. Vargas, R. Torres-Cadena, D.T. Reyes-Castillo, J. Rodríguez-Hernández, M. Gembicky, E. Menéndez-Proupin, D. Solis-Ibarra, Chemical diversity in lead-free, layered double perovskites: a combined experimental and computational approach. Chem. Mater. **32**(1), 424–429 (2020)